

EXPERIMENTAL AND NUMERICAL INVESTIGATION OF TRAILING EDGE FILM COOLING DOWNSTREAM OF A SLOT WITH INTERNAL RIB ARRAYS

P. Martini, A. Schulz

Institut für Thermische Strömungsmaschinen, Universität Karlsruhe
Kaiserstr.12, 76128 Karlsruhe, Germany.
patrick.martini@its.uni-karlsruhe.de, achmed.schulz@its.uni-karlsruhe.de

C.F. Whitney

ALSTOM Power Technology Centre,
Cambridge Rd, Whetstone, Leicester, LE8 6BH, UK.
chris.whitney@power.alstom.com

E. Lutum

MTU Aero Engines GmbH, Thermodynamic (TPWT)
Dachauer Str. 665, 80995 Munich, Germany
ewald.lutum@muc.mtu.de

ABSTRACT

To enhance turbine efficiency the trailing edge thickness of stators and blades needs to be as thin as possible. One limitation on the trailing edge thickness is the requirement to cool this life limiting region of the blade. One technique used to achieve a thin cooled trailing edge is that of a pressure side cutback with film cooling slots. There is a paucity of fluid and heat transfer data regarding this type of geometry which is currently being addressed by the EC funded Framework V project AITEB. This paper reports on experimental work being undertaken by the University of Karlsruhe and accompanying CFD calculations being performed by MTU Aero Engines and ALSTOM Power. Experimental and numerical data presented includes cutback surface film cooling effectiveness together with slot discharge coefficient values.

NOMENCLATURE

A [m ²]	area	L [mm]	char. length	Re [-]	Reynolds number
α [deg]	wedge angle	λ [W/(mK)]	thermal cond.	R _f [mm]	fillet radius
b _r [mm]	rib width	M [-]	blowing ratio	ρ [kg/m ³]	density
C _D [-]	discharge coeff.	m [kg/s]	mass flow rate	s [mm]	pitch
D _{hyd} [mm]	hydr. diameter	μ [Pas]	dyn. viscosity	T [K]	temperature
H [mm]	slot height	p [N/m ²]	pressure	t [mm]	lip thickness
h [W/(m ² K)]	heat transf. coeff.	π [-]	pressure ratio	u [m/s]	velocity
η [-]	effectiveness	q [W/m ²]	heat flux	x,y,z [m]	co-ordinates
κ [-]	ratio of spec. heats	R [J/(kgK)]	gas constant		

Subscripts

aw	adiabatic wall	f	isoenergetic	r1, r2	rib index
bl	boundary layer	hg	hot gas	tot	total
c	coolant	rad	radiative	w	wall
cond	conductive				

INTRODUCTION

Efficient operation of modern gas turbines results in turbine inlet temperatures which are significantly higher than the maximum allowed by the blade material. Therefore, appropriate cooling techniques are required to cool the blade and achieve the target life. Normally, the blades are cooled by a combination of convection and film cooling and therefore designed with internal cooling air passages. One of the most critical regions of the turbine blade is the trailing edge, which has, from aerodynamic aspects, to be as thin as possible. This causes an inherent conflict with cooling requirements as manufacturing difficulties emerge from the integration of internal cooling passages into the thin trailing edge region. One state-of-the-art cooling technique, which leads to particularly thin trailing edges, is obtained by cutting material from the pressure side of the trailing edge forming a characteristic step. The cutback uncovers the internal coolant passage creating a slot from which air can emerge to generate a cooling film on the trailing edge cutback. In order to increase the integrity of the trailing edge region, the structure has to be stiffened by ribs or pin-fin arrays located inside the internal cooling passage connecting the pressure and the suction side. These arrays work as turbulators to enhance the convective heat transfer in the cooling passage and control the blade cooling mass flow. Figure 1 shows a cross-sectional view of a turbine blade with pressure side trailing edge cutback.

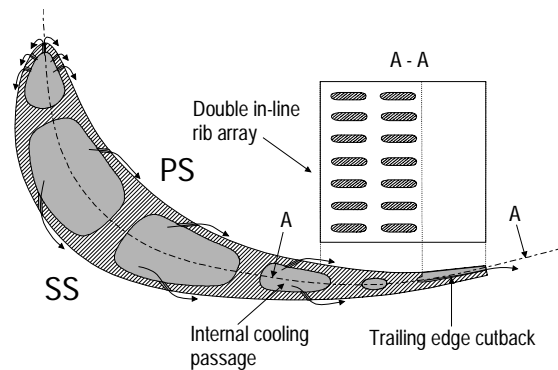


Figure 1: Cross sectional view of a turbine blade with pressure side trailing edge cutback.

There have been a number of publications dealing with two dimensional film cooling through slots (e.g. [1-4]), but so far the influence of rib or pin-fin arrays on film cooling has not been taken into account. The present work concentrates on the experimental and numerical investigation of a typical trailing edge configuration, where coolant ejects from a slot, disrupted by a double in-line rib array as shown in Figure 1. This work addresses the fundamental film cooling mechanism on the trailing edge cutback. Therefore possible additional influences due to Mach number variation or rotor-stator interaction were not considered here. However, Mach number effects are believed to be of small importance for the envisioned applications in the high subsonic to transonic range. Effects of rotor-stator interactions affect film cooling mainly through a variation of surrounding pressure level at the coolant exit. This slightly alters the blowing rate with time around a time mean value. The film cooling effectiveness levels of the investigated configurations are expected to show moderate variation with blowing rate variation, which in turn has little impact from the unsteady pressure fluctuations.

DESCRIPTION OF TEST FACILITY AND TRAILING EDGE MODEL

All experimental work was carried out on a scaled-up trailing edge model integrated into the atmospheric hot wind channel of the Institut für Thermische Strömungsmaschinen (ITS) at the

Universität Karlsruhe, Germany. Figure 2 shows a schematic view of the test facility and further details can be obtained from [5].

The trailing edge model investigated has been scaled up by a factor of 10 and consists of a double in-line rib array. Each row consists of 7 equally spaced ribs. The cooling slot has an overall width of 180 mm with the lateral distance between two ribs being 24 mm. In contrast to the first rib row, it was decided to provide the ribs in the second row with fillets in order to consider any influence due to the fillet radii on the flow field downstream the ejection slot.

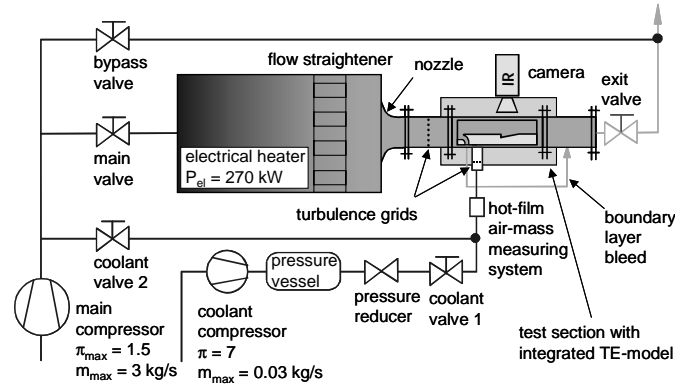
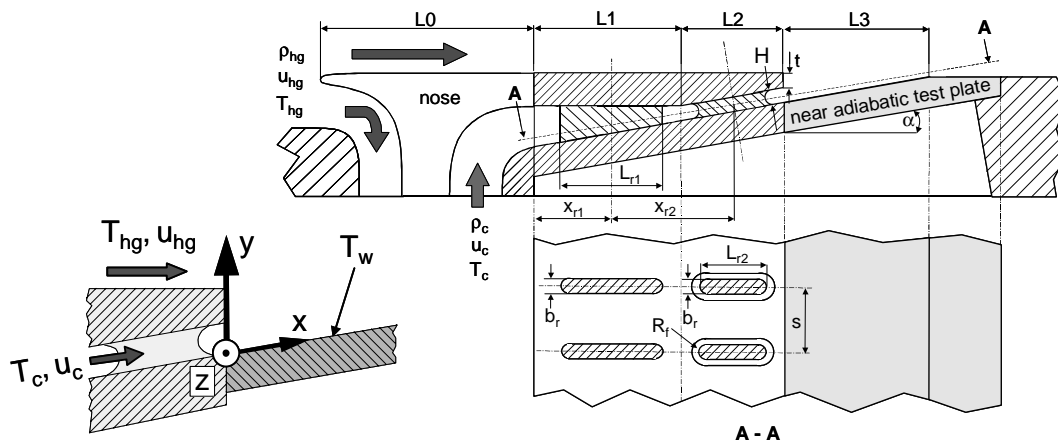


Figure 2: Schematic view of the atmospheric test facility

Figure 3 shows all main geometric details of the investigated trailing edge cooling configuration. For a realistic boundary layer thickness of the main flow, the wall affected hot gas was bled off by a variable boundary layer bleed so that a new boundary layer started to develop on the tip of the nose. A wire trip was used at the end of the nose region to achieve laminar/turbulent transition. To obtain Biot number similarity between the real engine configuration and the investigated model, the ribs and the pressure side walls were fabricated from high-grade steel with a thermal conductivity of around $\lambda = 16 \text{ W/(mK)}$. A low conductivity plastic material ($\lambda = 0.25 \text{ W/(mK)}$) was used for the test plate in the region of the pressure side trailing edge cutback to provide near adiabatic conditions for the determination of the film cooling effectiveness.



L0	L1	L2	L3	H	t	α	x_{r1}	x_{r2}	L_{r1}	L_{r2}	b_r	s	R_f
95	40	28	40	4	4	10	22	32	28	20	4	24	2

Figure 3: Schematic view of the trailing edge model with nomenclature (in [mm] or [deg])

BOUNDARY CONDITIONS AND MEASURING TECHNIQUE

Main Flow Conditions

Due to the scale factor used for the trailing edge model, it was not possible to obtain engine representative Mach and Reynolds numbers simultaneously. Therefore it was decided to perform all tests at realistic Reynolds numbers as compressibility effects were considered to be of minor importance compared to the influence of the Reynolds number. This has been indicated in previous research work performed at ITS, where the hot gas Mach number was found to have only a slight effect on film cooling effectiveness, as long as subsonic ($Ma < 1$) conditions are considered [6]. The Reynolds number of the main flow, Re_{hg} , was fixed at 250,000, where:

$$Re_{hg} = \frac{u_{hg} \cdot \rho_{hg} \cdot L}{\mu_{hg}} = \frac{u_{hg} \cdot \rho_{hg} \cdot (L0 + L1 + L2 + L3)}{\mu_{hg}} \quad (1)$$

The hot gas temperature was set at 500 K which led, in combination with the coolant air temperature, to an engine representative temperature ratio of around 0.62. The static pressure in the hot main flow was slightly above atmospheric. With $Re_{hg} = 250,000$ a velocity of around 45 m/s ($Ma = 0.1$) was obtained for the main flow. The main flow conditions were derived from a Pitot total pressure/temperature probe exposed to the main flow in the hot gas channel, while pressure taps in the lateral wall measured the main flow static pressure. To obtain an appropriate turbulence level a grid (square mesh array of square bars) was placed upstream of the nose tip which was calculated to generate a turbulent intensity of around 7 percent, at a macroscopic length scale of the order of 10 mm, on the trailing edge cutback [7].

Coolant Flow Conditions

Five different blowing ratios ($M = (\rho_c u_c) / (\rho_{hg} u_{hg})$) between 0.5 and 1.1 were tested leading to coolant Reynolds numbers, Re_c , of approximately 6,000 to 13,000. Re_c has been calculated using the hydraulic diameter D_{hyd} of the ejection slots formed by the last rib row in the L2 area (see Figure 3).

$$Re_c = \frac{u_{hg} \cdot \rho_{hg} \cdot M \cdot D_{hyd}}{\mu_c} \quad (2)$$

As for the main flow, a turbulence grid was inserted in the rectangular coolant duct providing at the inlet of L1 a turbulent intensity of around 5 percent, at a macroscopic length scale of the order of 1 mm. The coolant temperature was measured at two locations. At the first location, the inlet of L1, it ranged from 304 K up to 315 K, dependent on the coolant mass flow, and was measured using a hot film sensor. The second location, the ejection slot, marked the starting point of film cooling. The temperature measured at the ejection slot was chosen to be the reference coolant temperature for any film cooling effectiveness presented in this work.

Infrared Measuring Technique

In the study of three-dimensional flows where the local, two-dimensional, temperature distribution on the film cooled surface is of particular interest, IR-Thermography can be

applied very successfully. The main advantage of IR-Thermography is its high local resolution. In the present study, the infrared scanner THERMOVISION 900 by AGEMA was utilised with a maximum resolution of 136 x 272 pixels where each pixel represents an area of around 0.56 x 0.56 mm². Details of the IR measuring technique can be taken from [8]. The infrared data was calibrated by 9 thermocouples (0.5 mm diameter) embedded on the upper surface of the test plate. By applying this measurement technique a relative error of less than 1 percent for the wall temperature measurements was achieved.

Post Processing Scheme

The material for the test plate features a very low thermal conductivity ($\lambda = 0.25$ W/(mK)) but since it is not perfectly insulating, the surface temperature distribution on the trailing edge cutback was influenced by remnant heat fluxes which had to be accounted for. The wall heat fluxes were calculated by means of a finite volume (FV) calculation of the solid test plate where the surface temperatures around the plate were employed as boundary conditions. For the upper surface, the calibrated IR-data was used whereas 13 thermocouples provided sampling points for temperature interpolation on the remaining surfaces (front, end, bottom). Radiative heat transfer, caused by significant temperature differences between the film cooled trailing edge cutback and the hot surrounding channel walls, was also considered. The principles of the radiative heat transfer calculation have been described in [5]. The convective heat flux was found by subtracting the radiative heat flux from the calculated wall heat flux.

$$q_{\text{conv}} = q_w - q_{\text{rad}} = h_f \cdot (T_{\text{aw}} - T_w) \quad (3)$$

where h_f is the isoenergetic heat transfer coefficient of film cooling. Assuming constant flow properties (ρ , μ , λ), h_f can be taken as the heat transfer coefficient for the isoenergetic flow ($T_c/T_{\text{hg}} = 1$). The adiabatic film cooling effectiveness was determined by using the convective heat flux only, as follows:

$$\eta_{\text{aw}} = \frac{T_{\text{hg}} - T_{\text{aw}}}{T_{\text{hg}} - T_c} = \eta - \frac{q_{\text{conv}}}{h_f \cdot (T_{\text{hg}} - T_c)} \quad (4)$$

η is the (measured) diabatic film cooling effectiveness, which is in case of the near adiabatic experiment not far from η_{aw}

$$\eta = \frac{T_{\text{hg}} - T_w}{T_{\text{hg}} - T_c} \quad (5)$$

The isoenergetic heat transfer coefficient h_f was unknown in equation 4. It can be derived from the principle of superposition for film cooling by performing a second experiment with an altered wall temperature (by heating or cooling the wall) for constant flow conditions [9]. But, as η is not too far from η_{aw} , a reasonable estimation for h_f has been provided here.

EXPERIMENTAL RESULTS

Discharge Coefficient Results

The discharge coefficient C_D quantifies the global pressure loss for the internal coolant passage. It is defined by the ratio of the measured coolant mass flow and the ideal mass flow resulting from an isentropic expansion from the total pressure $p_{1,t}$ measured in front of L1 to

the static pressure p_2 of the main flow outside the ejection slot. The reference area, A_2 , is the total ejection area of the mere slot, i.e. continuous slot without ribs,

$$C_D = \frac{\dot{m}_{c,real}}{\dot{m}_{c,ideal}} = \frac{\dot{m}_{c,real}}{p_{1,t} \cdot \left(\frac{p_2}{p_{1,t}}\right)^{\frac{\kappa+1}{2\kappa}} \cdot A_2 \cdot \sqrt{\frac{2\kappa}{(\kappa-1) \cdot R \cdot T_{1,t}} \left[\left(\frac{p_{1,t}}{p_2}\right)^{\frac{\kappa-1}{\kappa}} - 1 \right]}} \quad (6)$$

All discharge coefficients were derived under the described main flow conditions. Figure 4 shows C_D values for varying Re_c . As the modular design of the existing trailing edge model allows the removal of ribs from the slot, the present configuration ($s/H = 6$) is compared to discharge coefficients obtained for the continuous slot geometry without ribs in L1 and L2. The ribbed configuration yields a significantly lower discharge coefficient than the continuous configuration. Typically, the discharge coefficients increase with increasing Re_c .

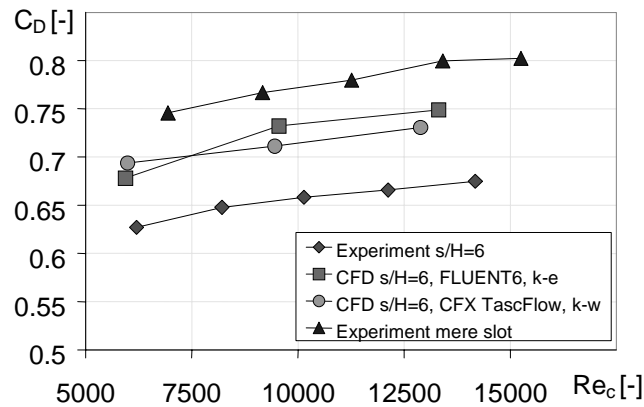


Figure 4: Discharge coefficients for the double in-line rib and continuous slot configurations for varying Re_c

Pressure Distribution along L2-Rib

For a more detailed view on the pressure distribution inside the coolant passage, one rib in the L2 region was instrumented with four additional pressure taps as shown in Figure 5. The pressure was related to the mass flow averaged total pressure in front of the first rib row and plotted over the four pressure tap locations (Figure 5).

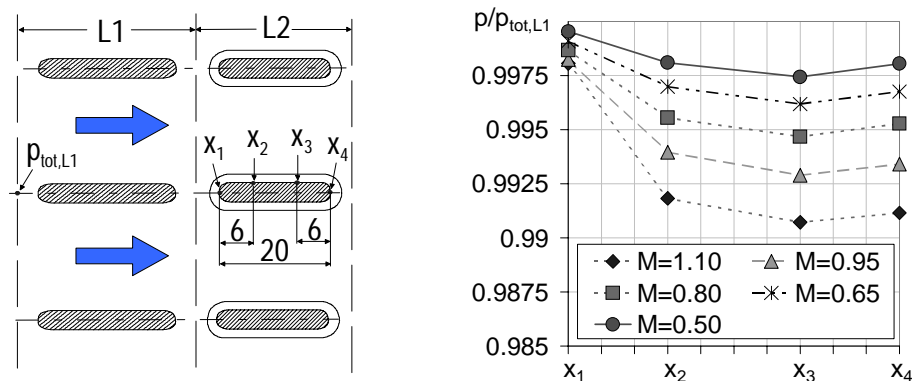


Figure 5: Measured pressure distribution along the second rib row for different M

In the region of the first rib row, the coolant accelerates as the flow area is decreased by the ribs and the converging coolant passage walls (see Figure 3). Flow separation downstream of the L1-ribs results in a significant production of turbulence leading to a decreased total pressure. As the first pressure tap (x_1) coincides with the L2 rib stagnation point, the plotted pressure ratio in Figure 5 quantifies the total pressure loss at the x_1 -location.

Entering the second rib row, the coolant flow accelerates slightly as the L2-ribs further decrease the flow area. The overall flow acceleration reduced the static pressure in the region of x_2 . Downstream, the measurements showed an additional static pressure decrease followed by a slight recovering at the end of the rib.

Film Cooling Effectiveness

The wall temperature distribution was measured on the trailing edge cutback (L3-region) by means of IR-Thermography. Figure 6 shows the distribution of film cooling effectiveness η (equation 5) downstream of the ejection slot for three different blowing ratios ($M=0.5$; $M=0.8$; $M=1.1$).

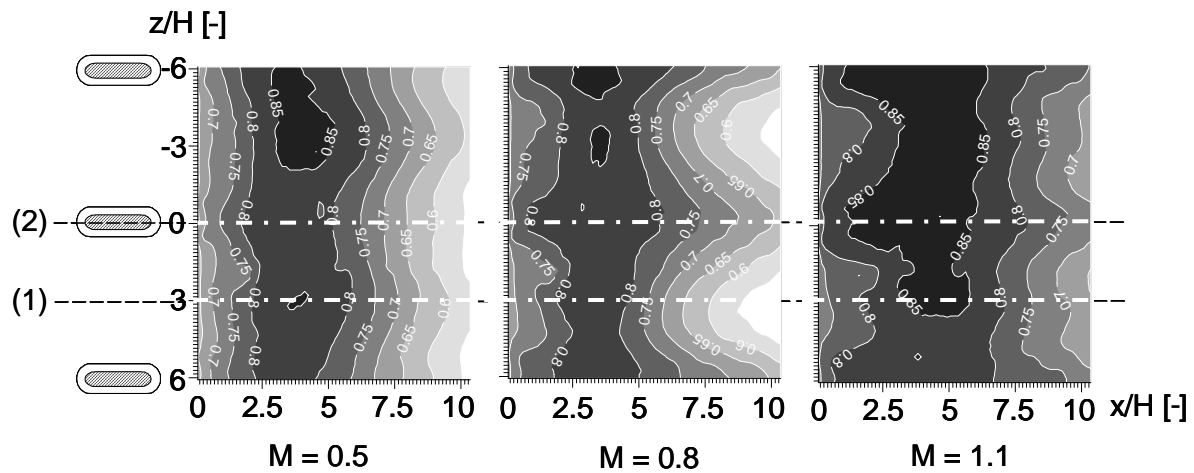


Figure 6: Measured film cooling effectiveness η on the trailing edge cutback for different blowing ratios (M)

Due to the influence of the ribs and depending on the blowing ratio, a two-dimensional distribution of the film cooling effectiveness results on the trailing edge cutback. In the lateral direction, for $M = 0.5$ and $x/H > 2.5$, the highest levels of film cooling effectiveness were located along the symmetry lines of the coolant passages which were laterally bounded by each two ribs (Figure 6 line (1)). The increase in blowing ratio to $M = 0.8$ led to a characteristic change of the η distribution on the trailing edge cutback indicating a strong influence of the ribs. Here, for constant x ($x/H > 5$), the maximum values were no longer located along the centrelines of the coolant passages but on the symmetry lines of the ribs (Figure 6 line (2)). In comparison to $M = 0.5$ it is interesting to note that there was no significant change of the total level of the film cooling effectiveness.

As the blowing ratio was further increased to $M = 1.1$ a higher overall film cooling effectiveness was measured on the trailing edge cutback but the qualitative distribution for ($x/H > 5$) was similar to that seen at $M = 0.8$. However, it seems that the effectiveness started to increase again in the region between the ribs (Figure 6 line (1)), so that the temperature distribution became more one-dimensional.

It must be noted that the region directly downstream of the ejection slot $0 < x/H < 2-3$ was influenced by thermal boundary layer effects due to remnant heat transport from the lower

walls (in L1 and L2) into the coolant flow. This led to the coolant temperature distribution qualitatively shown in Figure 7. This temperature distribution was locally measured directly at the ejection slot and at several different locations farther downstream by means of a traversing total temperature probe. Directly downstream of the ejection slot, on the near adiabatic test plate (L3-region), the wall temperature T_w was somewhat above the coolant core temperature T_c (used as the reference coolant temperature in equation 5) which resulted in reduced film cooling effectiveness. As mixing effects increase the uniformity of the coolant temperature on the near adiabatic surface, the wall temperature decreases in streamwise direction, leading to increased η -values. Downstream of a region of constant maximum film cooling effectiveness, η decreases again as the hot gas starts to influence the wall temperature on the near adiabatic test plate. It can be assumed that the thermal effects described above are finished when hot gas starts to influence the wall temperature. Due to radiation and remnant heat fluxes in the near adiabatic test plate, the measured (diabatic) film cooling effectiveness η is different from the adiabatic film cooling effectiveness, η_{aw} , which can be calculated using equation 4.

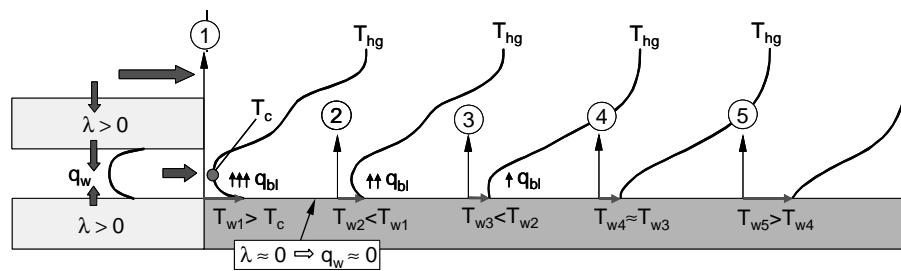


Figure 7: Influence on the wall temperature distribution by the thermal boundary layer of the coolant flow.

Figure 8 shows the laterally averaged adiabatic film cooling effectiveness over the non-dimensionalized downstream distance from the ejection slot (x/MH) for five different blowing ratios.

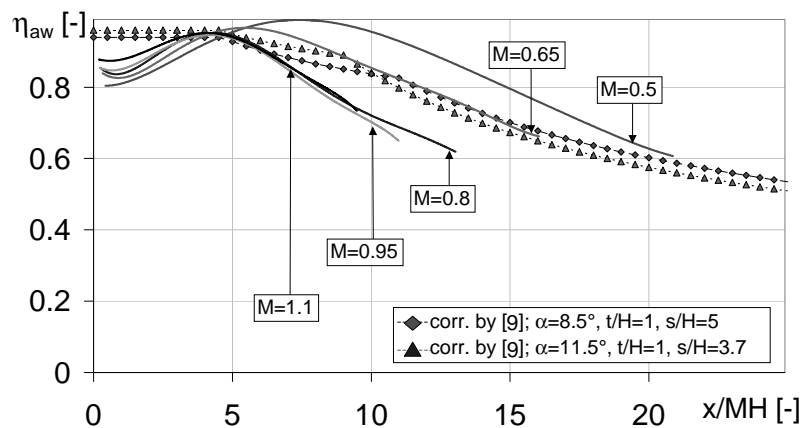


Figure 8: Adiabatic film cooling effectiveness η_{aw} downstream the ejection slot for different blowing ratios M .

In the near slot region all results show an increase of the laterally averaged adiabatic film cooling effectiveness caused by the described thermal boundary layer effects. For all blowing ratios the maximum of η_{aw} is close to unity and therefore 10 to 15 percent above the maximum measured values of η which emphasises the importance of the post processing procedure. The start of the hot gas affected wall region was found to be dependent on the

blowing ratio and ranges from $x/MH \approx 4.5$ for $M > 0.8$ over $x/MH \approx 5.5$ for a blowing ratio of $M = 0.65$ to $x/MH \approx 8$ for $M = 0.5$. All curves show a similar decrease of the adiabatic film cooling effectiveness with increasing x/MH . The curves of η_{aw} match each other for $M > 0.8$ whereas reducing the blowing ratio leads to increased η_{aw} in Figure 8. As already stated, for $M < 0.8$ a higher amount of coolant mass flow does not result in a significantly increased local adiabatic film cooling effectiveness for the investigated range of x/H . In fact, the laterally averaged adiabatic film cooling effectiveness for $M = 0.8$ is slightly lower than for $M = 0.5$ in the range of $x/H < 9$. The results of the adiabatic film cooling effectiveness were compared to correlations from the literature. Taslim *et al.* [10], investigated the film cooling effectiveness for slots of various exit geometries. The correlations shown in Figure 8 are based on two trailing edge geometries closest to the current investigated configuration. The configurations reported in [10] did not contain any ribs but had evenly spaced pieces of land reaching from the internal coolant passage to the very end of the trailing edge which were flush with the pressure side wall.

The two correlations result in slightly different values of η_{aw} both of which are well inside the range of η_{aw} obtained in this work. For $M = 0.65$ the present values of η_{aw} fit the correlations very well whereas lower as well as higher blowing ratios result in significant deviations from what is predicted by both correlations. However it seems that in case of higher x/MH the results for $M = 0.5$ seem to converge with the correlations.

NUMERICAL RESULTS

The trailing edge geometry studied experimentally by the University of Karlsruhe has also been investigated numerically by industrial partners of the AITEB consortium. ALSTOM Power have performed supporting CFD studies using the commercial code FLUENT 6.0 with mesh generation being performed using the FLUENT mesh generator GAMBIT 2.0. Use was made of the 'journal' files created by Gambit to create a template to simplify and speed up the mesh generation of the trailing edge geometry. Further details of the development and capabilities of the mesh template process can be found in [11]. The mesh created was 2.3 million cells in size and had an unstructured hybrid mesh with hexahedral cells in the hot gas path and trailing edge cutback region and tetrahedral cells within the cooling passage. A boundary layer mesh was applied to all wall surfaces with sufficient resolution to ensure that $y^+ < 1$ in all regions except very close to the hot gas inlet.

The mesh created for the $s/H = 6$ configuration consisted of one periodically repeating pitch of the ribbed geometry in the lateral direction with the two axial ribs located centrally within this lateral region. The hot gas inlet and cooling flow inlet were modelled using a velocity inlet boundary condition. The exit was modelled as a static pressure outlet boundary condition. To minimise the computational domain only approximately half the height of the hot gas path was modelled. Hence, the top surface of the computational domain was specified as symmetric and this was demonstrated to be the case during the commissioning phase of the experimental facility. The wall defining region L3 was modelled as adiabatic whilst all other walls, including both rib surfaces had a uniform temperature of 380 K. Figure 9 shows the computational domain and boundary regions whilst further details of boundary conditions are given in the Table within Figure 10. The realisable k- ϵ turbulence model was specified for the solution with the mainstream inlet turbulence intensity set at 7 percent and the coolant turbulence intensity set at 5 percent. These values are consistent with the experimental values and the numerical studies performed by MTU.

Discharge Coefficient Results

The discharge coefficient for the present configuration ($s/H = 6$) have been determined using the expression given in equation 6. The predicted fluid pressure, temperature and coolant mass flow rate have been extracted from the CFD analysis to determine the discharge coefficient. As can be seen in Figure 4 the CFD analysis over predicts the experimental C_D values by 8-12 percent for the Reynolds number range considered. This discrepancy may be due to turbulence production generated by the gap between the two axial ribs being under-predicted, resulting in a lower pressure drop across the ribs than measured. Considering the low pressure drop across this cooling passage the level of agreement is considered to be reasonable. The effect of this would be less coolant flow to the trailing edge region leading to possible failure of the turbine blade unless the discrepancy was accounted for in the design process.

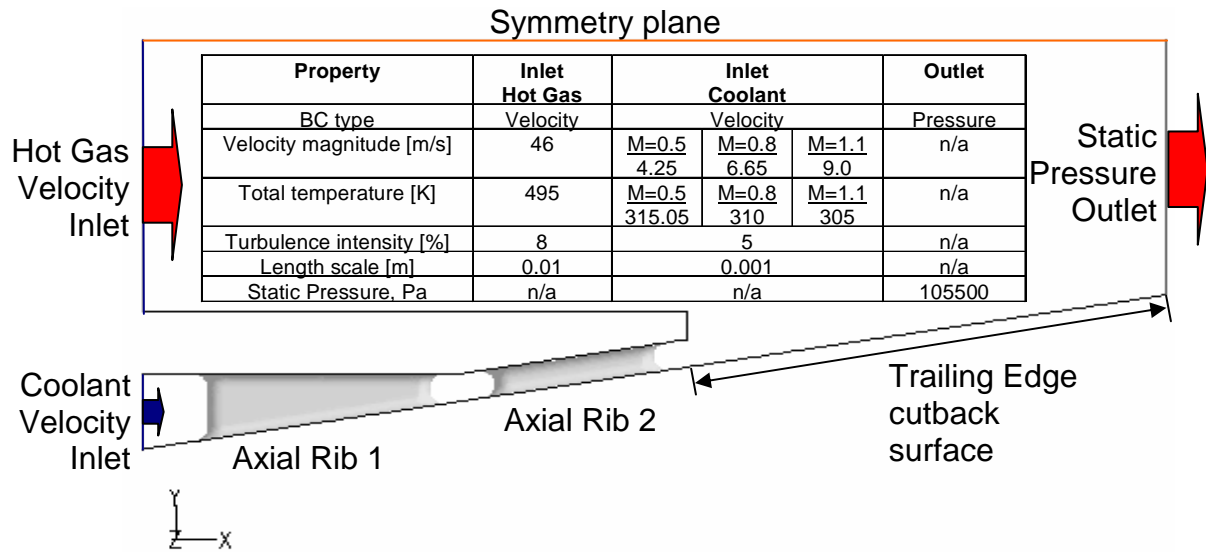


Figure 9: Schematic side view of fluid domain used in CFD analysis and table of boundary conditions.

Effectiveness Results

Figure 10 shows contour plots of adiabatic film cooling effectiveness plotted on the same scale for three blowing rates studied.

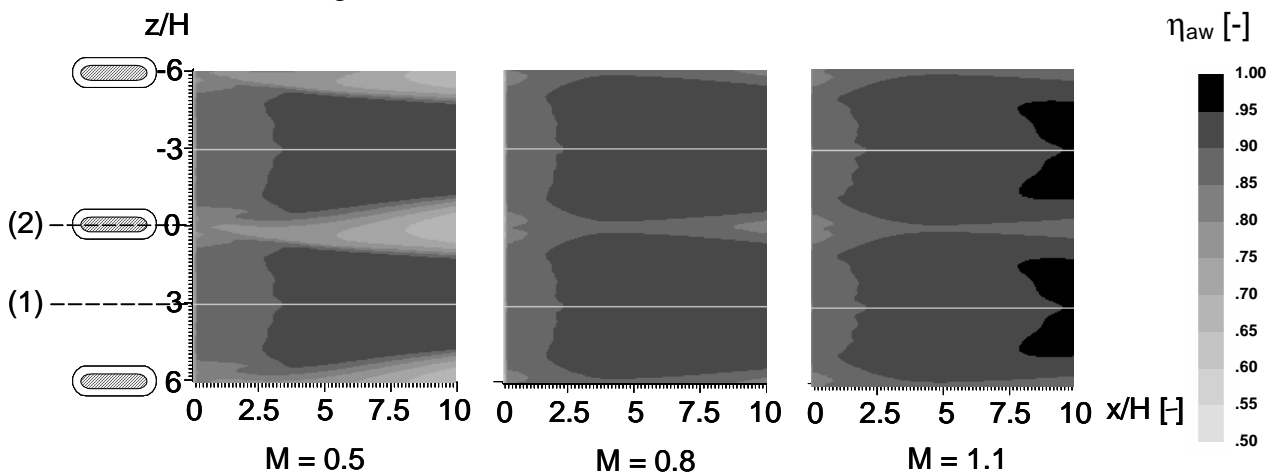


Figure 10: CFD predictions of cooling effectiveness for blowing rates $M = 0.5, 0.8$ and 1.1 .

Comparison with the experimental results shown in Figure 6 reveal that there are some important differences between the two sets of data. For $M = 0.5$ the regions of low cooling effectiveness behind the ribs are much more prominent than the experiments reveal. This may be due to under prediction of the mixing in the lateral direction. In all three cases the peak effectiveness occurs between the ribs and as the blowing rate increases the x/H position of the peak moves further rearward. It can be seen that there is little difference in the effectiveness pattern and magnitude between $M = 0.8$ and 1.1 . For $M = 1.1$ the influence of the rib is slightly less than for $M = 0.8$ but the change to a one dimensional effectiveness pattern as seen in the experimental results is not evident.

Similar numerical investigations have been performed by MTU Aero Engines. These investigations were conducted with CFX-TASCflow by using multi-block structured meshes, which were built with ICEM CFD Hexa. The same computational domain as mentioned before (Figure 9) was considered. However, in this study only one half pitch of the cooling channels was modelled, i.e. the region between (1) and (2) as indicated in Figure 11. A symmetry boundary condition has been applied for both of these planes. Figure 11 shows the multi-block structured mesh with 0.89 million cells that was used. In general a value of $y^+ < 2$ could be achieved, which was required by the applied $k-\omega$ baseline model. Identical boundary conditions as those summarised in Table 1 have been applied during these calculations.

The comparison of the predicted pressure loss inside the cooling passages with the corresponding measurements and FLUENT prediction is shown in Figure 4 and indicates a fairly good agreement between experimental and numerical results. The predicted discharge coefficients are consistently approximately 10 percent greater than corresponding measurements.

A comparison of predicted and measured laterally averaged adiabatic film cooling effectiveness values is also shown in Figure 11 for above mentioned target blowing rates $M = 0.5, 0.8$ and 1.1 . The distributions indicate the streamwise development of the cooling film downstream from the ejection slot (x/H). The characteristic increase in the film cooling effectiveness distributions, due to the thermal boundary layer effects, were captured by the TASCflow predictions. However the predicted location of the maximum of η_{aw} is shifted towards greater x/H values compared to the experimental results, i.e. for $M = 0.5$ to $x/H \approx 8$, for $M = 0.8$ to $x/H \approx 10$ and for $M = 1.1$ to $x/H \approx 11$. In addition the predictions indicate in contrast to the experiments a continuous increase of film cooling effectiveness with increasing blowing rate and a less strong decrease of film cooling effectiveness downstream of these maximum locations. It can be concluded that the qualitative behaviour has been fairly well captured by these simulations. However for η_{aw} quantitative differences in the range of 0.1 to 0.3 could be observed, which might lead to significant over prediction of the film cooling effectiveness particularly close to the trailing edge of the blade.

Holloway et al. [12] investigated recently a similar pressure side bleed configuration with a view to examine an “unusual behaviour” that was found in corresponding experiments. This addressed behaviour was also observed in the current measurements, i.e. for $M < 0.8$ an increase of cooling mass flow achieved not an increase of film cooling effectiveness as usually expected for slot film cooling. From the 3-D steady results in [12], it was determined that unsteady simulations needed to be performed. Holloway et al. [13] conducted 2D unsteady calculations and show that the vortex shedding off of the lip was the key mechanism that caused the previously unexplained experimental results.

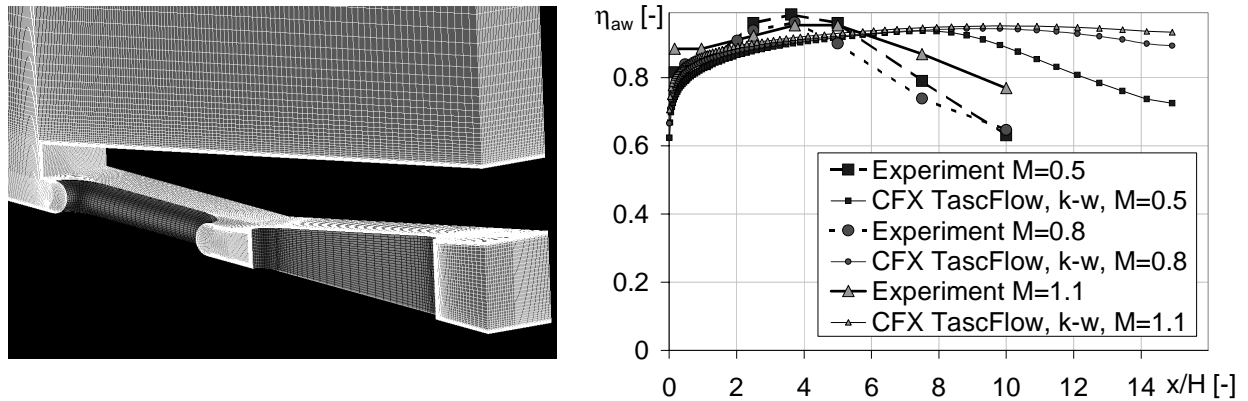


Figure 11: Multi-block structured mesh and comparison of measured and predicted laterally averaged film cooling effectiveness values for blowing rates $M=0.5$, 0.8 and 1.1 .

SUMMARY AND CONCLUSIONS

Detailed experimental and numerical studies have been presented for a modern trailing edge configuration with a double in-line rib array.

For the investigated blowing ratios, the discharge coefficients of the cooling configuration are in the range of 0.65 and, as expected, increase with the Reynolds number. They were found to be slightly over-predicted by CFD but, when considering the extremely low pressure ratio which drives the coolant flow, deviations of around 10 percent seem to be still acceptable.

The experimental results on film cooling effectiveness on the trailing edge cutback indicate that the ribs have a considerable influence on the local and laterally averaged adiabatic film cooling effectiveness. The laterally averaged values of η_{aw} have been compared to two correlations by [10]. Although the results obtained by the correlations lie well inside the measured range, there exists a tendency that lower blowing ratios are under-predicted whereas increased blowing ratios are over-predicted by the correlations.

The numerical results on the adiabatic film cooling effectiveness show significant deviations to the measurements, which indicate that the highly complex turbulent mixing process is still not captured correctly by CFD. Some of the most recent numerical studies indicate that the flow field downstream of the ejection slot is highly unsteady due to periodic vortex shedding. As this could be responsible for increased mixing of hot gas and coolant which has been seen in the experiments, future work will deal with the consideration on these unsteady effects in CFD in order to predict more realistic results on adiabatic film cooling effectiveness.

ACKNOWLEDGEMENTS

The reported work was performed as part of the European Union funded project “Aero-thermal Investigation of Turbine Endwalls and Blades” (AITEB, 5FP, G4RD-CT-1999-00055). The permission for the publication is gratefully acknowledged by the authors. The last author would like to thank Mr. V. Roch for conducting the CFX-TASCflow calculations.

REFERENCES

- [1] R. J. Goldstein, Film Cooling: Advances in Heat Transfer, Vol. 7 , pp 321-379, 1971
- [2] S. Sivasegaram, J.H. Whitelaw, Film Cooling Slots: the Importance of Lip Thickness and Injection Angle, J. Mech. Eng. Sci., Vol. 7, pp 22-27, 1969
- [3] D. K. Mukherjee, Film Cooling with Injections through Slots, Transactions of ASME, J. of Eng. for Power, Vol. 7 , pp 556-559, 1976

- [4] W. K. Burns, J.L. Stollery, The Influence of Foreign Gas Injection and Slot Geometry on Film Cooling Effectiveness, *Int. J. Heat Mass Transfer* Vol. 12 , pp 935-951, 1969
- [5] S. Baldauf, A. Schulz, S. Wittig, High Resolution Measurements of Local Effectiveness by Discrete Hole Film Cooling, *ASME Paper 99-GT-46*, 1999
- [6] M. Gritsch, Experimentelle Untersuchungen zum aerothermischen Verhalten nicht-zylindrischer Filmkühlbohrungen, Ph.D.-Thesis, Institut für Thermische Strömungsmaschinen (ITS), Universität Karlsruhe (TH), 1998
- [7] P. E. Roach, The generation of nearly isotropic turbulence by means of grids, *Heat and Fluid Flow*, Vol. 8 No. 2, pp 83-92, 1987
- [8] M. Martiny, R. Schiele, M. Gritsch, A. Schulz, S. Wittig, In Situ Calibration for Quantitative Infrared Thermography, *QIRT 96*, Eurotherm Seminar Nr. 5, pp 3-8, 1996
- [9] H. Choe, W. M. Kays, R. J. Moffat, The Superposition Approach to Film-Cooling, *ASME Paper*, 74-WA/HT-27, 1974
- [10] M.E. Taslim, S.D. Spring, B.P. Mehlmann, An Experimental Investigation of Film Cooling Effectiveness for Slots of Various Exit Geometries, *AIAA Paper 90-2266*, 1990
- [11] P. Martini, A. Schulz, S. Wittig, Entwicklung eines Verfahrens zur Generierung vollständig parametrisierter, dreidimensionaler CFD-Rechengitter am Beispiel konvektiv-filmgekühlter Turbinenschaufelhinterkanten, *DGLR Jahrestagung*, 2002
- [12] D. S. Holloway, J. H. Leylek and F. A. Buck, Pressure-Side Bleed Film Cooling: Part I Steady Framework for Experimental and Computational Results, *ASME-Paper GT-2002-30471*, 2002.
- [13] D. S. Holloway, J. H. Leylek and F. A. Buck, Pressure-Side Bleed Film Cooling: Part II Unsteady Framework For Experimental and Computational Results, *ASME-Paper GT-2002-30472*, 2002.